Dehydroxylation of Phosphate Laser Glass

C. B. Thorsness, T. I. Suratwala*, R. A. Steele, J. H. Campbell
University of California, Lawrence Livermore National Laboratory, 7000 East Avenue, L-500, Livermore, California 94550
J. S. Hayden, S. A. Pucilowski
Schott Glass Technologies Inc., 400 York Ave., Duryea, PA 18642
K. Suzuki
Hoya Corporation USA, 3400 Edison Way, Fremont, CA 94538

Rates of dehydroxylation of two Nd-doped metaphosphate laser glasses (LG-770 and LHG-8) are measured and modeled. Glass melts ranging in size from 100 g to 2.8 kg were bubbled with O_2 containing various H_2O partial pressures (P_{H_2O}) and with O_2/Cl_2 mixtures at temperatures ranging from 925-1300°C. The OH content in the glass was measured by monitoring the OH absorption at 3.333 μm at various bubbling times. The OH removal by inert gas bubbling (e.g. O_2 bubbling) is governed by the transport (diffusion) of OH to the glass liquid/vapor interface and by the chemical equilibrium between OH at the surface and H_2O in the gas phase. The equilibrium OH content in glass melts bubbled with O_2 containing different P_{H_2O} varies as $P_{H_2O}^{1/2}$. Reactive gas dehydroxylation (using Cl_2 bubbling) is enhanced by the reverse Deacon reaction where Cl_2 gas reacts with H_2O in the gas phase to form HCl. A time-dependent, one-dimensional bubble-column dehydroxylation model is developed and used to describe the rates of dehydroxylation for glasses. The model uses measured or literature values for the diffusion coefficient of OH in the melt (D_{tOH}), the H_2O/OH equilibrium constant (K_w), and the equilibrium constant for the reverse Deacon reaction (K_d). The model does a good job simulating/predicting dehydroxylation rates of small-scale test melts and production-scale continuous melting operations.

Keywords: dehydroxylation, dehydration, phosphate laser glass, O_2 / Cl_2 bubbling, glass melting, reverse Deacon reaction, bubble column

1. INTRODUCTION

Rare earth-doped glasses, such as Nd^{3+} and Er^{3+} in silicate and phosphate glasses, are used in a wide variety of applications ranging from high power laser systems to fiber or planar waveguide amplifiers [1-7]. The presence of hydroxyl (OH) groups quenches the fluorescence of the rare earth ion, which reduces laser gain and adversely affects laser performance [2]. In the case of Nd^{3+}, this quenching transfers energy from the upper laser level ($^4F_{3/2}$ state of Nd^{3+}) to the second vibrational overtone of OH [2]. For most laser applications, it is desirable to reduce the OH concentration to <200 ppm [8].

The H_2O and OH present in the raw materials and the H_2O present in the environment are the source of OH in manufactured glass. A variety of techniques can be employed to reduce the amount of OH in the glass that include: 1) thermal drying of raw materials (i.e. calcining); 2) addition of non-reactive dehydroxylation agents; and 3) addition of reactive dehydroxylation agents.

The thermal drying of the raw materials is simply performed by calcining the powder before melting. However, it is still difficult to remove all hydroxyls from the powders, and the small residual amounts often lead to 100-1000 ppm OH levels in the final glass. Non-reactive dehydroxylation is commonly performed by bubbling inert gases through a melt (e.g. O_2, N_2) [1, 9-15]. Reactive dehydroxylation involves reaction between a halide (such as Cl and F) with OH or H_2O. Two common methods that have been utilized are exposing a porous glass preform to Cl_2 gas or bubbling a glass melt with Cl_2 gas[12-17]. Other reactive agents (solids, liquid or gases) can also be used [18].

Despite the great general interest in the dehydroxylation of glasses, surprisingly little is understood or published about details of the mechanism and kinetics. In the present paper, we explore the rate of dehydroxylation using O_2 and Cl_2 bubbling in glass melts of two commercial Nd-doped phosphate laser glasses (LG-770 from Schott Glass Technologies Inc. and LHG-8 from Hoya Corporation USA). First, the results for the OH content of glass melts bubbled with O_2 containing

* Correspondance: Suratwala1@llnl.gov; Telephone: 925-422-1884; Fax:925-423-0792

various H_2O partial pressures (P_{H_2O}) and with O_2/Cl_2 mixtures at various temperatures, melt sizes, bubbling flow rates, and cover gas flows are reported (Section 3). Next, we describe a proposed mechanism of dehydroxylation (Section 4.1) which involves three steps: (1) mass transport of OH to the melt/vapor interface; (2) thermal dehydroxylation (governed by H_2O/OH equilibrium), and (3) reactive Cl_2 dehydroxylation (governed by H_2O/HCl equilibrium). Then, a description of the one-dimensional, time-dependent, bubble-column dehydroxylation model is given (Section 4.2). Specifically, we discuss the governing balance equations for the model and the relationships describing mass transfer at the bubble and top surface interfaces. Also, the limiting cases of the model are described. Finally, in Section 5, we apply the model to experimental melt data and discuss how the various experimental parameters affect the dehydroxylation kinetics, and how well the model describes the dehydroxylation kinetics for both small-scale test melts and production-scale continuous melting operations.

2. EXPERIMENTAL

Two commercial glasses, LG-770 (from Schott Glass Technologies, Inc.) and LHG-8 (from Hoya Corporation, USA) were used in the melting experiments. The base glasses are near meta-phosphate glasses, which have the molar compositions of (58-62)P_2O_5-(6-10)Al_2O_3-(20-25)K_2O-(10-15)MgO-(0-2)Nd_2O_3 for LG-770 and (55-60)P_2O_5-(8-12)Al_2O_3-(13-17)K_2O-(10-15)BaO-(0-2)Nd_2O_3 for LHG-8. The starting materials for each of the melts were either pre-made glass cullet or the raw materials which when melted have the compositions described above.

Three series of glass melts were conducted. The first series of glass melts, called H_2O/OH equilibrium melts, were conducted to determine the equilibrium amount of OH in the glass with different amount of H_2O in a bubbling gas stream. These melts were conducted by bubbling O_2 containing varying P_{H_2O} into a glass melt until equilibrium was reached in the melt. The second series of glass melts were performed to examine the dehydroxylation rates of LHG-8 glass; this was performed by bubbling dry O_2 gas into the glass melts and then measuring the OH content as a function of time. The third and final series of glass melts was performed to measure the dehydroxylation rates of LG-770 glass. These melts were bubbled with dry O_2 or O_2/Cl_2 gas mixtures and the OH content was measured as a function of time.

2.1 H_2O/OH Equilibrium melts

A schematic of the experimental setup used to perform the H_2O/OH equilibrium melts is shown in Fig. 1. Approximately 100 g of crushed glass cullet (LG-770 or LHG-8) was melted in a Pt crucible (250-ml capacity, 3-cm diameter) within a box furnace (Thermolyne 1400 or 47900) at temperatures ranging from 925°C to 1200°C; a round Pt sheet (10-cm diameter with a 1.0-cm hole) was used as a cover for the crucible. A quartz tube was dipped into the glass melt through a hole at the top of the furnace, and O_2 gas enriched with various H_2O partial pressures (P_{H_2O}) was bubbled into the melt. P_{H_2O} was established by bubbling dry O_2 gas (-57°C dew point) through a fritted tube in a water bath set to temperatures ranging from 3.5°C to 29.7°C. A portion of the gas was fed into an optical dew point sensor (General Eastern Model 1311DR) which measured the actual P_{H_2O} (see Fig. 1). The Cu lines were heated by heating tape to avoid water condensation in the lines. Bubbling in the glass melt was performed for 2-4 hours, typically at a flow rate of 5 standard ft^3/h (scfh). After bubbling, the quartz tube was removed and the glass melt was poured into steel molds ($4 \times 4 \times 1$ cm^3) coated with boron nitride (preheated to 550°C). The mold was then placed into an annealing furnace (Thermolyne 1500) set at 550°C and cooled at a rate of 60°C/h. The OH content in the glass samples was measured by cutting the samples into 0.5-2.0-mm slices and measuring the 3000 cm^{-1} (3.333 μm) transmission in a FTIR spectrometer (Perkin Elmer Spectrum 2000). The OH content is reported as OH absorptivity (α in cm^{-1}). The OH content of the starting cullet was low (~2 cm^{-1}) for all melts. The samples from the melts are identified as L-1 to L-31.

2.2 LHG-8 dehydroxylation melts

LHG-8 raw materials (2.8 kg) was placed into a fused quartz crucible (11 cm diameter × 17.5 cm depth) preheated in a resistively-heated furnace at temperatures ranging from 1000°C to 1165°C. A fused quartz square plate ($15 \times 15 \times 0.7$ cm^3) with a 1.0-cm hole in the center was used as a cover for the crucible. After heating for one hour, approximately 30 g of the melt was poured into a graphite mold ($4 \times 4 \times 1$ cm^3) preheated to 490°C. The mold was then stored in an annealing furnace set at 490°C. This first scoop sample represents the zero bubbling time sample (t = 0 h). The crucible was then reinserted into the furnace, and a fused silica tube (8-mm OD, 4-mm ID) was inserted into the glass melt through the hole in the fused quartz cover. O_2 was then bubbled at various flow rates ranging from 0.54 to 1.1 scfh. Note no cover gas was used. Scoop samples were taken at various bubbling times (0.5, 1, 1.5, 2, and 3 hours). All six scoop samples were placed within an

annealing oven and cooled at a rate of 30°C/h to room temperature. The OH content of the resulting samples were measured in the same manner as described above. These melts are labeled as H-1 to H-4.

2.3 LG-770 dehydroxylation melts

LG-770 glass cullet with high OH content ($\alpha = 45\ cm^{-1}$) was used in these melting experiments. The cullet weighing 1.0 kg or 1.8 kg was placed in a quartz crucible (9.4-cm ID × 13-cm or 21-cm height) and inductively heated to temperatures between 1100°C to 1300°C. A 2.1-cm thick refractory brick was used to cover the crucible. The first scoop sample was taken after 20-25 minutes of melting the cullet; this was designated as time zero. Then a 0.8-cm OD quartz tube was submerged 8 cm into the melt through a hole in the refractory block. O_2 or O_2/Cl_2 gas mixture was passed through at various flow rates (0.27 to 1.1 scfh). A cover gas (O_2, 10 scfh, dew point = -62°C, P_{H_2O} = 0.025 mmHg) was supplied through another 0.8 cm OD quartz tube through a different hole in the refractory block to prevent outside humid air from entering the melt system. Scoop samples were taken at various bubbling times and poured into steel molds holding ~60 g of glass. The glasses were annealed at 550°C and cooled to room temperature at 30°C/h. The OH content of the resulting samples was measured in the same manner as described above, and the resulting melts are labeled S-12 to S-42.

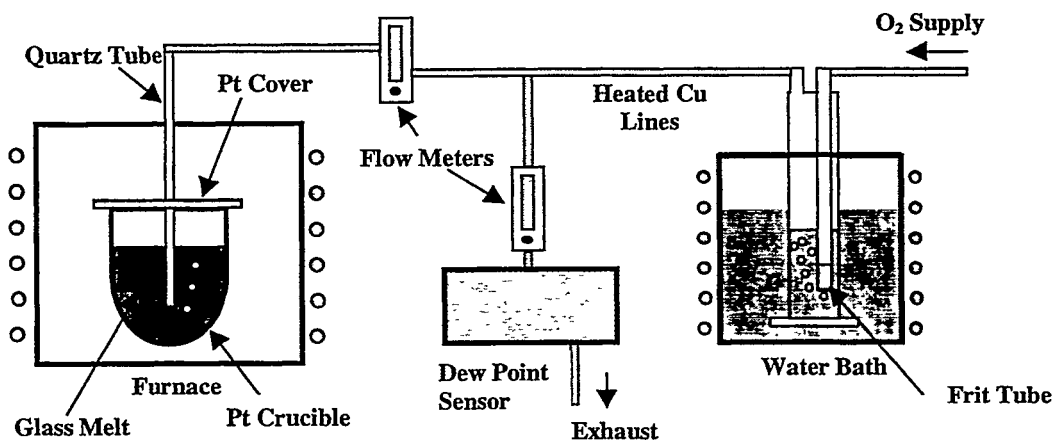

Fig. 1. Schematic of experimental setup used for the H_2O/OH equilibrium melts.

3. RESULTS

The results of the test melts to evaluate the equilibrium relation between C_{gH_2O} (H_2O concentration in the gas phase) and $C_{\ell OH}$ (OH concentration in the liquid melt) are summarized in Table 1. The first four melts (L-1 to L-4) were conducted at various O_2 bubbling flow rates ranging from 0.2 to 8 scfh to determine the flow rate required to prevent interaction of the melt surface with the outside humidity (see Fig. 2). O_2 bubbling of 5 scfh or greater gave an OH content in the final glass that did not change, suggesting that the melt had reached equilibrium and was not affected by the outside atmospheric humidity. Hence the remaining H_2O/OH equilibrium melts (L-5 to L-27) were conducted at bubbling flow rates of 5 scfh. P_{H_2O} in the bubbling gas varied from 6 Pa (–57°C dew point) to as high as 4100 Pa (+29.7°C dew point). As expected, an increase in P_{H_2O} resulted in an increase in OH content in the glass. Also, at higher temperatures, the equilibrium was driven toward lower OH level in the glass.

The results of the dehydration melts by O_2 or O_2/Cl_2 bubbling are summarized in Table 2. Also shown are the melt parameters (glass composition, temperature, melt geometry, cover gas flow, bubbling flow rate, and gas composition) and the resulting OH content of the scoop samples taken at various bubbling times.

Table 1: Summary of H_2O/OH equilibrium experiments

Melt #	Glass	Melt Temp. (°C)	Melt Size (g)	O_2 Bubbling rate (scfh)	Bubbling time (h)	α (cm^{-1})	P_{H_2O} (Pa)	K_{wp} ($Pa^{1/2}/cm^{-1}$)
Variable bubbling rate								
L-1	LHG-8	1100	100	0.4	2	4.6	6	na
L-2	LHG-8	1100	100	2	2	0.8	6	
L-3	LHG-8	1100	100	5	2	0.4	6	
L-4	LHG-8	1100	100	8	2	0.4	6	
Variable water vapor pressure & temperature								
L-5	LHG-8	925	100	5	2	4.20	6	
L-6	LHG-8	925	100	5	2	17.20	638	
L-7	LHG-8	925	100	5	2	25.30	1184	1.40
L-8	LHG-8	925	100	5	2	29.60	1756	
L-9	LHG-8	1000	100	5	4	1.10	6	
L-10	LHG-8	1000	100	5	4	16.00	625	
L-11	LHG-8	1000	100	5	2	18.70	927	
L-13	LHG-8	1000	100	5	4	23.20	1131	1.63
L-14	LHG-8	1000	100	5	2	26.50	1942	
L-15	LHG-8	1000	100	5	4	27.80	2008	
L-16	LHG-8	1100	100	5	2	1.00	6	
L-17	LHG-8	1100	100	5	2	13.80	798	
L-18	LHG-8	1100	100	5	2	18.60	1330	1.96
L-19	LHG-8	1100	100	5	2	25.00	2328	
L-20	LG-770	1050	100	5	2	2.88	6	
L-21	LG-770	1050	100	5	2	29.50	1915	1.48
L-22	LG-770	1100	100	5	2	0.90	6	
L-23	LG-770	1100	100	5	2	18.80	971	1.56
L-24	LG-770	1100	100	5	2	29.10	1968	
L-25	LG-770	1200	100	5	2	2.20	6	
L-26	LG-770	1200	100	5	2	17.10	1250	2.01
L-27	LG-770	1200	100	5	2	27.20	2939	
L-28	LG-770	1300	1000	0.5	2.5	9.65	610	
L-29	LG-770	1300	1000	0.5	2.5	23.13	2980	
L-30	LG-770	1300	1000	0.5	6	29.89	3990	2.18
L-31	LG-770	1300	1000	0.5	6	30.38	4100	

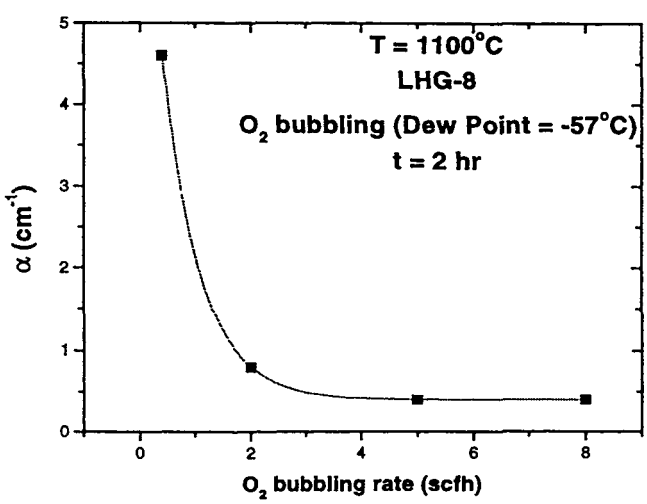

Fig. 2. OH content in LHG-8 laser glass as function of O_2 bubbling rate during melting. (100 g melts, T = 1100°C, t = 2 h). The line represents a single exponential fit added as a guide to the eye.

Table 2: Summary of dehydration experiments by O_2 or O_2/Cl_2 bubbling.

Melt #	Glass Type	Melt Diam and height (cm)	Melt Temp (°C)	Cover Gas Flow (scfh)	Total Bubble Flow (scfh)	Bubble Flow (% Cl_2)	Scoop sampling time: 0 h	0.5 h	1.0 h	1.5 h	2.0 h	2.5 h	3.0 h	4.0 h	6.0 h
							α (cm^{-1})								
H-1	LHG-8	11 x 12.7	1100	0	0.54	0	141	115	99.9	87.2	76.1		59.2		
H-2	LHG-8	11 x 12.7	1100	0	1.1	0	139	76.6	73.9	61.9	51.0		37.4		
H-3	LHG-8	11 x 12.7	1000	0	1.1	0	154	126	99.6	85.8	73.8		47.6		
H-4	LHG-8	11 x 12.7	1165	0	1.1	0	153	87.4	72.4	55.9	43.5		34.5		
S-12	LG-770	9.4 x 8.5	1300	20	0	0	34.7	22.6		8.48		6.34			
S-13	LG-770	9.4 x 8.5	1300	20	0.5	0	36.1		6.71						
S-14	LG-770	9.4 x 8.5	1300	20	0.5	0	34.8				4.57				
S-31	LG-770	9.4 x 8.5	1300	20	0.54	21.2	46.6	4.35	0.70	0.51				0.46	0.41
S-32	LG-770	9.4 x 8.5	1250	20	0.54	21.2	48.9	5.47	0.85		0.44			0.39	0.32
S-33	LG-770	9.4 x 8.5	1200	20	0.54	21.2	48.5	6.80	0.92		0.51			0.46	0.41
S-34	LG-770	9.4 x 8.5	1300	20	0.52	11.0	44.2	10.7	2.60		0.73			0.68	0.39
S-35	LG-770	9.4 x 8.5	1300	20	0.57	33.7	43.4	3.65	2.65		0.63			0.56	0.39
S-36	LG-770	9.4 x 8.5	1300	20	0.50	0.0	46.4	8.43	2.82		1.53			0.90	0.73
S-37	LG-770	9.4 x 8.5	1300	20	1.08	21.2	46.7	3.13	1.24		0.73			0.41	0.41
S-38	LG-770	9.4 x 17.0	1300	20	1.08	21.2	42.1	2.45	1.19		0.41				
S-39	LG-770	9.4 x 17.0	1300	20	0.54	21.2	42.3	6.66	1.41		0.46				
S-40	LG-770	9.4 x 17.0	1200	20	1.08	21.2	47.8	6.22	1.31		0.46				
S-41	LG-770	9.4 x 17.0	1200	20	0.27	21.2	45.6	17.3	6.78		1.29				
S-42	LG-770	9.4 x 17.0	1200	20	0.54	21.2	46.9	11.5	3.52		0.70				

4. DEHYDROXYLATION MECHANISM AND MODEL

4.1 Mechanism

The glass compositions of the two phosphate glasses used in this study (listed in experimental section) both have near meta-phosphate compositions (O/P ~3). The basic structure of phosphate glasses has been well studied, and near-metaphosphate glasses can be described structurally as linear phosphate chains [19]. Molten phosphate glass readily reacts with H_2O which is believed to hydrolyze a P–O–P bond creating two chain terminating P–OH bonds [15, 20]. For dehydroxylation to occur, the reverse reaction takes place at a liquid/gas interface (such as the bubble or top surface interface).

The detailed mechanism describing dehydroxylation of phosphate laser glass is not well understood. However, we have had reasonable success in analyzing dehydroxylation data using a model that assumes the two most important aspects of the dehydroxylation process involve 1) a mass transport step and 2) two chemical equilibrium constraints. This is shown schematically in Fig. 3.

The transport step (step 1 in Fig. 3) is the diffusion of the OH carrying component from the bulk glass melt to a melt/vapor interface. The migrating species is likely a proton [21]; however for simplicity we treat the diffusion as an effective OH migration which is characterized by an effective OH diffusion coefficient (D_{tOH}). We assume that the mass transport rate is proportional to the gradient in the OH concentration. D_{tOH} has been previously measured for LG-770 at temperatures ranging from 200-1000°C [22]; an empirical fit to the data gives

$$D_{tOH} = \left(2.09\frac{m^2}{\text{sec}}\right)\exp\left(\frac{-3.45\times10^4}{T} + \frac{8.0\times10^6}{T^2}\right), \quad (2)$$

where T is the temperature in K.

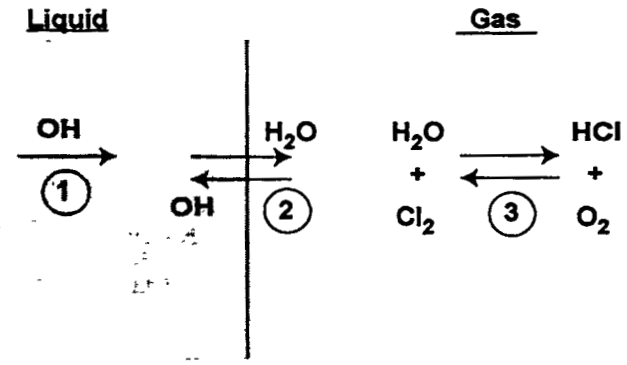

(1) **Mass transport to liquid surface ($D_{\ell OH}$)**

$$(P\text{-}OH)_\ell \longrightarrow (P\text{-}OH)_s$$

(2) **H_2O/OH Equilibrium**

$$2(P\text{-}OH)_S \rightleftharpoons P\text{-}O\text{-}P)_\ell + H_2O_g$$

$$K_w = \frac{\sqrt{C_{gH_2O}}}{C_{\ell OH_S}}$$

(3) **H_2O/HCl Equilibrium**

$$2H_2O + 2Cl_2 \rightleftharpoons 4HCl + O_2$$

$$K_d = \frac{C_{gHCl}{}^4 \, C_{gO_2}}{C_{gH_2O}{}^2 \, C_{gCl_2}{}^2}$$

Fig. 3. Schematic of liquid melt / gas interface illustrating the proposed physical and chemical processes that govern thermal and chemical dehydroxylation.

At the interface, which may be the exposed top surface of the melt or a bubble surface, it is assumed that the governing reaction is [2]

$$2\left(\begin{array}{c} O \\ \| \\ -P-OH \\ | \\ O^- \end{array}\right)_s \leftrightarrow H_2O + \begin{array}{c} O \\ \| \\ -P-O- \\ | \\ O^- \end{array} \begin{array}{c} O \\ \| \\ P- \\ | \\ O^- \end{array} \quad , \tag{3}$$

where the OH concentration at the gas/liquid interface ($C_{\ell OH_s}$ in mol/m^3) is in equilibrium with the water concentration in the gas phase (C_{gH_2O} in mol/m^3) according to the equilibrium relation:

$$K_w = \frac{\sqrt{C_{gH_2O}}}{C_{\ell OH_s}} \quad , \tag{4}$$

where K_w is the equilibrium constant ((mol/m^3)$^{-1/2}$). Because these reactions take place at high temperatures, kinetics for reaction (3) are assumed to be so fast that the material concentrations can be described by chemical equilibrium.

If the bulk melt has obtained equilibrium with C_{gH_2O}, then the surface OH concentration ($C_{\ell OH_s}$) is equal to the bulk OH concentration ($C_{\ell OH}$). However, we can only measure the bulk OH content by optical absorption (α). Then by the same token, when the bulk equilibrium has been reached, then $\alpha = \alpha_s$ where α_s is the absorption coefficient for OH at the surface. Therefore the surface equilibrium relation given by Eq. (4) is more conveniently given as

$$K_{wp} = \frac{\sqrt{P_{H_2O}}}{\alpha_s} \quad , \tag{5}$$

and when bulk equilibrium is reached, it is given by

$$K_{wp} = \frac{\sqrt{P_{H_2O}}}{\alpha} \quad . \tag{6}$$

The values for K_{wp} as a function of temperature can be determined from the H_2O/OH equilibrium melts (see Table 1). When α is plotted versus $P_{H_2O}^{1/2}$, it yields a straight-line for both LG-770 and LHG-8 suggesting Eq. 6 is valid (see Figs. 4a and b). The reciprocals of the line slopes in Figs. 4a and b give values for K_{wp} which are reported in the last column of Table 1. At higher temperatures, the slopes are lower which leads to higher K_{wp} values. In other words, the equilibrium OH content of the glass is lower at higher temperatures. At an equivalent temperature, the equilibrium OH content of LHG-8 is slightly lower than LG-770. This is shown in Fig. 4c where both glasses are compared at 1100°C (K_{wp} = 1.96 $Pa^{1/2}/cm^{-1}$ for LHG-8 and K_{wp} = 1.56 $Pa^{1/2}/cm^{-1}$ for LG-770).

Figure 4d is an Arrhenius plot of the equilibrium constant (K_{wp}) determined for both glasses; a linear fit to the data gives the expression

$$K_{wp} = K_o \exp\left(\frac{-\Delta G}{RT}\right) , \tag{7}$$

where ΔG is the free energy, K_o is the pre-exponential constant, and R is the ideal gas constant. The two glasses are found to have similar free energies (28.9 kJ/mol (LG-770) and 26.0 kJ/mol (LHG-8)), and the values for K_O are 20.4 $Pa^{1/2}/cm^{-1}$ (LG-770) and 19.14 $Pa^{1/2}/cm^{-1}$ (LHG-8).

In the presence of Cl_2, a vapor phase reaction between Cl_2 gas and H_2O vapor occurs,

$$2\,H_2O + 2\,Cl_2 \rightarrow 4\,HCl + O_2 \quad . \tag{8}$$

As written (left to right), Eq. (8) is known as the reverse Deacon reaction [23], with the Cl_2 acting to dehydrate the vapor. The equilibrium constant for this reaction is given by

$$K_d = \frac{C_{gHCl}^{\ 4}\, C_{gO_2}}{C_{gH_2O}^{\ 2}\, C_{gCl_2}^{\ 2}} \quad , \tag{9}$$

where C_{gO_2} , C_{gHCl} , C_{gCl_2} are the O_2, HCl, and Cl_2 concentrations in the gas phase (mol/m^3), and K_d is the equilibrium constant (mol/m^3). The equilibrium constant for Eq. (9) has been reported as [23]:

$$K_d = \frac{(10^{\frac{-6104}{T}+7.099}) \bullet atm}{RT} . \tag{10}$$

K_d has a value of 3996 and 7463 mol/m^3 at 1100°C and 1200°C, respectively [23]. These relatively large K_d values lead to low concentrations of water vapor in equilibrium mixtures. As a consequence, in systems containing chlorine in the bubbling gas, the driving force for mass transfer between the bulk glass and the glass/bubble interface remains high (i.e. $C_{\ell OH_s}$ is low). In contrast, in systems where only O_2 is present, the bubbles tend to reach saturation because of the equilibrium imposed by Eq. (5). In this case, the driving force for transport of OH out of the melt becomes small (i.e. $C_{\ell OH_s}$ is high), and the dehydration rate is correspondingly slower.

Although the details of the reaction mechanism between Cl_2 and H_2O are not well known, it is likely that Cl_2 dissociates to form Cl radicals at these high temperatures [16]. Regardless of the mechanism, the overall reaction can still be described by Eq. (8). Note also that the current model assumes that the potential reaction of OH at the glass interface with Cl or Cl_2 is negligible.

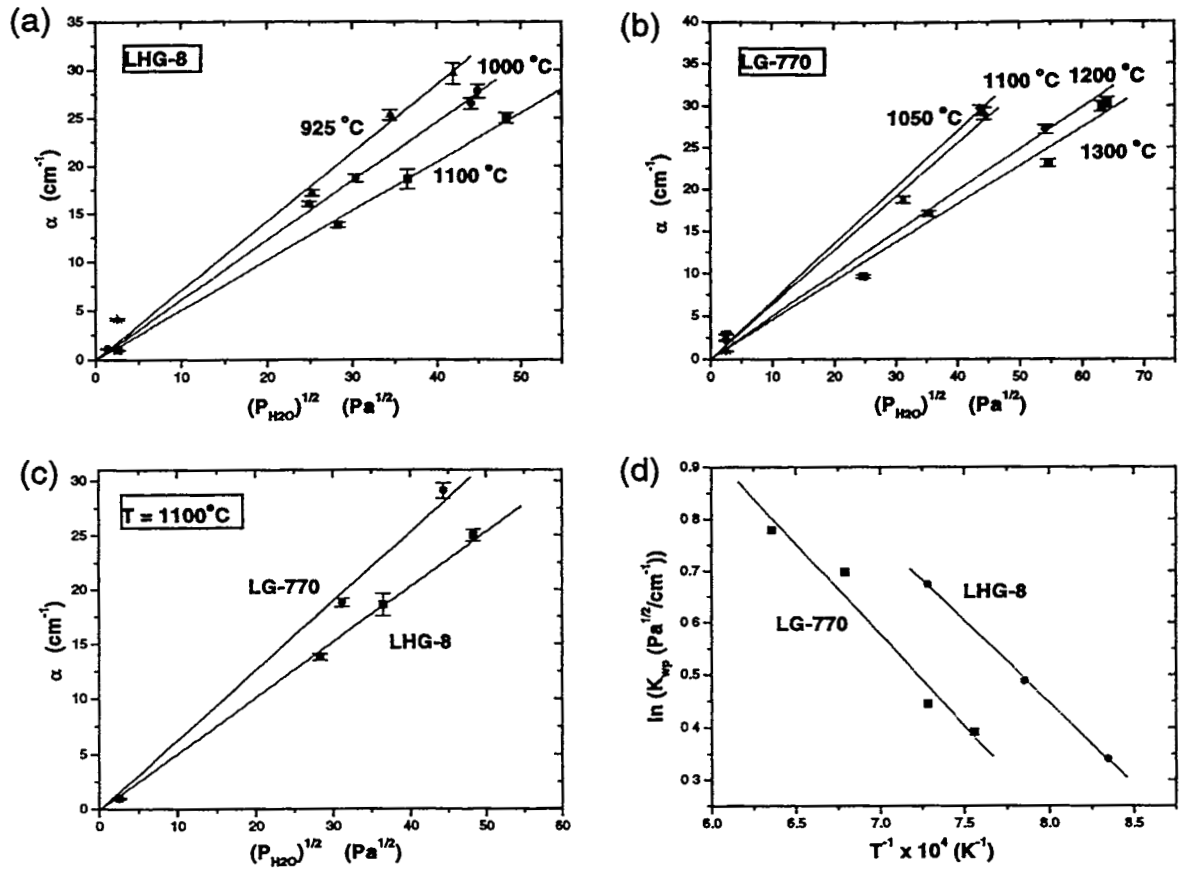

Figure 4. (a) OH content (α) as a function of the $P_{H_2O}^{1/2}$ for LHG-8 glass melts at various temperatures. The melting conditions and data points are reported in Table 1. The lines represent fits to the data where the inverse of the slope is K_{wp}. (b) Same as (a) for LG-770 glass melts. (c) OH content (α) as a function of the $P_{H_2O}^{1/2}$ at 1100°C for both glasses. (d) Arrhenius plot of the determined K_{wp} values (points) at various temperatures for LG-770 and LHG-8. The lines represent fits to the data points using Eq. (9).

4.2 Model Description

4.2.1 Balance Equations

A computer model has been developed that describes the removal rate of OH groups from phosphate laser glass using either an inert (e.g. O_2) or reactive (e.g. Cl_2) gas employing mass transfer constraints and reaction equilibriums discussed in the previous section. The model assumes the system can be described by equations appropriate for a time-dependent, one-dimensional bubble column (see Fig. 5).

The concentration of species (e.g. H_2O, OH, Cl_2, O_2 etc) in this model can be described mathematically by a system of coupled partial differential equations where the concentration is both a function of time (t) and height (z) in the bubble column. The generic set of equations used to describe a time-dependent, one-dimensional bubble column are simply the balance equations of each of chemicals species of interest in the gas and liquid phase [24]:

$$\frac{-\partial C_\ell}{\partial t} = E_\ell \frac{\partial^2 C_\ell}{\partial z^2} - U_\ell \frac{\partial C_\ell}{\partial z} - \frac{kA_b}{1-\phi}\left(C_\ell - C_\ell^*\right) - R_\ell \tag{11}$$

$$\frac{-\partial C_g}{\partial t} = E_g \frac{\partial^2 C_g}{\partial z^2} - U_g \frac{\partial C_g}{\partial z} + \frac{kA_b}{1-\phi}\left(C_\ell - C_\ell^*\right) - R_g \tag{12}$$

The subscript ℓ represents parameters or species in the liquid phase and g represents parameters or species in the gas phase. C is the concentration of particular species at time (t) and height (z), C* is the gas/liquid interface concentration, E is the

dispersion coefficient (m^2/sec), U is the average velocity (m/sec), kA_b is the overall mass transport (sec^{-1}), ϕ is the melt porosity, and R is the source or sink term from bulk reaction (mol/m^3 sec). Equations (11) and (12) state that the net flux of a particular chemical species at a certain time and height in the bubble column is determined by transport of species in and out of plane Z by dispersion (or diffusion) (first term on right-hand side of Eqs. (11) and (12)), by transport of species in and out of plane Z by convection (second term), mass transport to another phase (from liquid to vapor or vapor to liquid) (third term), and by the change in concentration from reaction with other species (fourth term). Using several assumptions, the balance equations can be simplified for the case of glass dehydroxylation. First, we assume that the liquid phase (i.e. the glass melt) is well mixed because gas bubbling is used in the melt. This means that the concentration of the liquid does not change with position, and therefore, all the liquid dispersion terms $\left(E_\ell \frac{\partial^2 C_\ell}{\partial z^2}\right)$ and the convection terms $\left(U_\ell \frac{\partial C_\ell}{\partial z}\right)$ for each of the chemical species go to zero. Secondly, the gas concentration as a function of position is dominated by convection (not diffusion), hence $E_g \frac{\partial^2 C_g}{\partial z^2} = 0$. Finally, we assume there is no bulk reaction in the liquid phase, $R_\ell = 0$. With the following constraints, the balance equations for OH in the liquid and H_2O in the gas phase can be written as:

$$\frac{-\partial C_{\ell OH}}{\partial t} = -\frac{kA_b}{1-\phi}\left(C_{\ell OH} - C_{\ell OH_s}\right) \tag{13}$$

$$\frac{-\partial C_{gH_2O}}{\partial t} = -U_g \frac{\partial C_{gH_2O}}{\partial z} + \frac{kA_b}{2\phi}\left(C_{\ell OH} - C_{\ell OH_s}\right) - R_{H_2O/HCl} \tag{14}$$

where $R_{H_2O/HCl}$ is the reaction rate of the reverse Deacon reaction (Eq. 8) which is given by:

$$R_{H_2O/HCl} = r_d \left(C_{gCl_2}\right)^2 \left(C_{gH_2O}\right)^2 \tag{15}$$

where r_d is the reaction rate constant for the reverse Deacon reaction. The balance equations can also be written for other chemical species (Cl_2, O_2, and HCl) in a similar manner as was done for H_2O and OH.

The dehydroxylation model treats all the balance equations, and numerically solves the set of partial differential equations. The H_2O/OH equilibrium constraint is imposed by using Eq. (4) and the computed gas phase H_2O concentration to set $C_{\ell OH_s}$. In the gas phase, the H_2O/HCl equilibrium is imposed by defining a simple mass action rate for the reverse Deacon reaction (Eq. (15)) which is fast. A rate for the forward reaction is defined using this rate and the equilibrium relation given by Eq. (9). In the model, competition between these rates enforces the H_2O/HCl equilibrium.

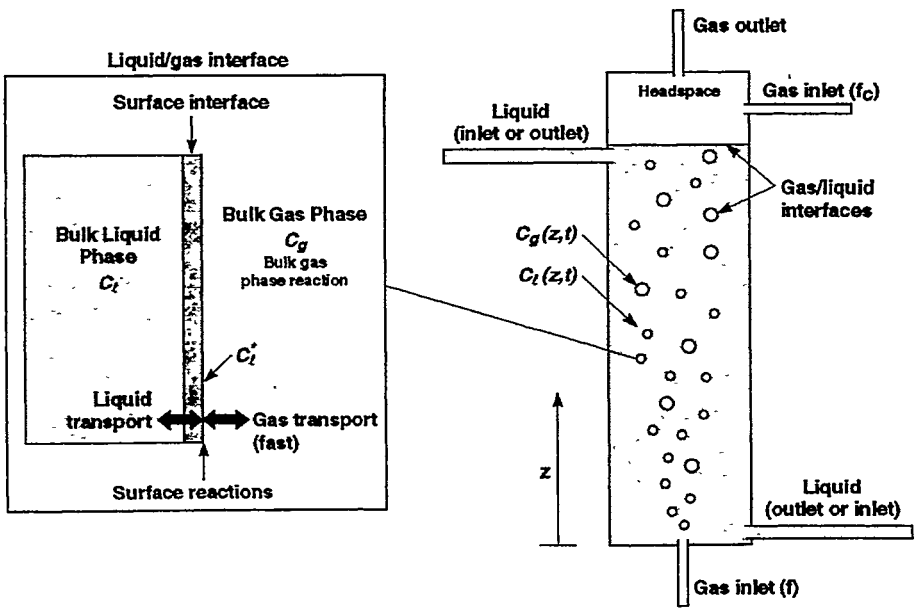

Fig. 5. Physical representation of the time-dependent, one-dimensional dehydroxylation model for OH removal using gas bubbling through a phosphate glass melt. The model treats both inert and reactive gases.

4.2.2 Mass transport at the melt/vapor interface

Transport of OH can occur at two types of interfaces, the bubble and top surface of the melt. When bubbles are formed in a bubble column, a large distribution of bubble sizes is typically observed. Hence there is not a simple representation of the interfacial area. Transport at the bubble interface is characterized in the model by an effective transport parameter, kA_b, which is the product of the mass transfer coefficient, k, and the interfacial area of the bubbles per unit volume, A_b. There are a large number of approaches and correlations used to estimate transport between the vapor phase inside a bubble and a surrounding liquid. The approach taken is dictated by the type of bubbling regime present. Bubbling regimes are often categorized by the nature of the bubble flow:

1. Homogeneous regime - Low bubble concentrations where the bubbles tend to move from the their origin to the surface with little interaction.
2. Heterogeneous regime - Moderate bubble concentrations where considerable interaction between bubbles occur.
3. Slug flow regime - Relatively high gas throughputs where large slugs of vapor and liquid are present.

We have chosen to use a bubble mass transfer correlation proposed by Deckwer [25] which can be employed over a large range of flow conditions. The effective bubble mass transfer is defined as

$$kA_b = \frac{D_{\ell OH} Sh}{d_c^2} \tag{16}$$

where d_c is the diameter of the bubble column (m), and

$$Sh = 0.6\, Sc^{0.5}\, Bo^{0.62}\, Ga^{0.31}\, \varphi^{1.1}. \tag{17}$$

The four dimensionless numbers appearing in Eq. (17) are the Sherwood (Sh), Schmidt (Sc), Bond (Bo) and Galilei (Ga) numbers, where

$$Sc = \frac{\mu_\ell}{\rho_\ell D_{\ell OH}},\quad Bo = \frac{g d_c^2 \rho_\ell}{\sigma},\ \text{and}\ \ Ga = \frac{g d_c^3 \rho_\ell^2}{\mu_\ell^2}. \tag{18-20}$$

Here μ_ℓ is the liquid viscosity (Pa sec), ρ_ℓ is the liquid density (kg/m^3), σ is the surface tension (N/m) of the liquid melt, and g is the acceleration of gravity (m/sec^2).

The fourth term in Eq. (17) is the melt porosity, ϕ, or void volume created by the bubbling. For viscous fluids Deckwer suggests using the following correlation to obtain the porosity,

$$\phi = 0.2\, Bo^{-0.13}\, Ga^{0.11}\, Fr^{0.54}. \tag{21}$$

Here *Fr* is the Froude number and is given by

$$Fr = \frac{u_g}{\sqrt{g d_c}}, \tag{22}$$

where u_g is the superficial gas velocity (m/s) which is given by

$$u_g = \frac{4 f RT}{\pi P d_c^2} \tag{23}$$

where f is the gas flow in mol/sec and P is the total gas pressure (Pa). Notice the correlation makes no explicit use of bubble diameter or rise velocity, nor does it compute these values. However, Eq. (16) does allow the necessary transport parameter kA_b, for the bubble interfaces, to be computed. Also, note that the superficial gas velocity (u_g) is just the average velocity (U_g) divided by the melt fraction ($1-\phi$).

By substituting Eqs. (17)-(23) into Eq. (16) the following dependence of the transport factor on process variables is obtained

$$kA_b \propto d_c^{-0.05}\, u_g^{0.6}\, D_{\ell OH}^{\ 0.5}\, \rho_\ell^{0.84}\, \mu_\ell^{-0.36}\, \sigma^{-0.48}. \tag{24}$$

Based on this correlation, one sees that the transport factor is a very weak function of vessel diameter, increases as superficial gas velocity or diffusivity increases and decreases as viscosity or surface tension increases.

The transport to/from a liquid column to an overlying gas at the top of a bubble column has received little attention in the literature because for many systems it is not important. However, in small systems it can be as important as the bubble phase transport. Unfortunately, we do not know of any established correlations for estimating surface transport coefficients from system variables. Consequently, we have employed a simple correlation using surface renewal theory which introduces two parameters surface velocity, v_s, and a characteristic length, l_s. Surface renewal theory can be used to relate these parameters and diffusivity to the transport coefficient at the surface is

$$k = \sqrt{\frac{4 D_{\ell OH}\, v_s}{\pi\, l_s}} \,. \tag{25}$$

Parameterized in this fashion it is possible to make at least limiting estimates of the magnitude of the transport by choosing reasonable values of v_s and l_s. Notice, however, that the transport coefficient actually depends only on the ratio of these two parameters.

As mentioned above, the characterization of the surface transport is the most difficult to deal with. In the following, we assume that l_s is a measure of the activity of bubbles breaking at the surface and that this activity is proportional to the flux of gas in the bubbles, with higher flux leading to more violent action and thus a smaller effective length scale. We further assume that this behavior can be approximated using the simple relation

$$l_s = \frac{L_s}{u_g}, \tag{26}$$

where L_s is a constant. Since the surface transport actually depends on the ratio of v_s and l_s (Eq. (25)), we choose a reasonable but arbitrary value for v_s (0.3 m/sec), a value equal to the rise velocity of the larger bubbles in the system. We allow L_s to be a parameter to be determined by fitting of model results to the experimental data.

4.2.3 Limiting cases

The partial differential equations described in Section 4.2.1 can only be solved numerically. However, it is instructive to explore limiting cases where the differential equations yield analytical solutions. For example, if the system is limited only by mass transfer of OH in the liquid to the liquid/vapor interface, the following equation applies:

$$\frac{dC_{\ell OH}}{dt} = -\frac{kA_V}{1-\phi} C_{\ell OH} \,. \tag{27}$$

Here it is assumed that the equilibrium constant K_w is sufficiently large, or sufficient chlorine is present, such that the effective equilibrium concentration of OH at the vapor/liquid interface ($C_{\ell OH_s}$) is zero. Equation (27) can be easily integrated giving:

$$\frac{C_{\ell OH}}{C_{\ell OH_o}} = \exp\left[-\frac{kA_V}{1-\phi} t\right] \,. \tag{28}$$

A simplified set of equations can also be developed for the case in which transport is fast and the system is controlled by the two previously defined equilibrium relations. This is done by writing the overall hydrogen balance for the system:

$$V(1-\phi)\frac{dC_{\ell OH}}{dt} = -f\left(2y_{H_2O} + y_{HCl}\right) \,. \tag{29}$$

where V is the melt volume. y_{H_2O} and y_{HCl} are gas mole fractions of H_2O and HCl, respectively, exiting the system. For simplicity we assume that no H_2O or HCl enter the system in the gas phase. Using the ideal gas law and Eq. (9) and (4), the gas mole fractions can then be described as:

$$y_{H_2O} = \frac{C_{gH_2O}}{C_g} = \frac{RT\, K_w^{\,2}\, C_{\ell OH}^{\,2}}{P} \,, \tag{30}$$

$$y_{HCl} = \frac{C_{gHCl}}{C_g} = \frac{RT K_w C_{\ell OH}}{P}\left(\frac{K_d C_{gCl_2}^{\ 2}}{C_{gO_2}}\right)^{1/4} \tag{31}$$

where P is the total gas pressure (Pa). Note, because mass transfer is fast, $C_{\ell OH} \approx C_{\ell OH_s}$. Combining the equilibrium relations with this hydrogen balance gives

$$\frac{dC_{\ell OH}}{dt} = -\frac{f RT}{PV(1-\phi)}\left(2K_w^{\ 2} C_{\ell OH}^{\ 2} + \left(\frac{K_d C_{gCl_2}^{\ 2}}{C_{gO_2}}\right)^{1/4} K_w C_{\ell OH}\right). \tag{32}$$

If no chlorine is present ($C_{gCl_2} = 0$) then Eq. (32) can be integrated to give the result

$$\frac{1}{C_{\ell OH}} = \frac{1}{C_{\ell OH_o}} + \frac{2f K_w^{\ 2} RT t}{PV(1-\phi)}. \tag{33}$$

In cases where significant amounts of Cl_2 are present and the water vapor levels in the exiting gas are small compared to the HCl levels, the right hand side of Eq. (32) will be dominated by the second term in the bracket. In this case Eq. (32) can be integrated to give

$$\frac{C_{\ell OH}}{C_{\ell OH\,o}} = \exp\left[\frac{-f RT K_w}{PV(1-\phi)}\left(\frac{K_d C_{gCl_2}^{\ 2}}{C_{gO_2}}\right)^{1/4} t\right]. \tag{34}$$

Notice that in the presence of Cl_2, the form of the equation describing the evolution of OH levels in the melt has the same exponential form for both the mass transfer controlled (Eq. (28)) and the equilibrium controlled (Eq. (34)) cases. In either case, if data are plotted on a semi-log plot a straight line should result if the limiting case applies. In one case the slope of the line would be proportional to the overall transport coefficient, whereas in the other case it yields information on the magnitude of the equilibrium constants.

On the other hand, in the absence of chlorine, a semi-log plot of the data would only be a straight line if the system were dominated by mass transport (Eq. (28)). If equilibrium constraints dominate the system then a plot of the reciprocal of OH concentration versus time would yield a straight line (Eq. (33)). Table 3 summarizes the limiting cases described in this section.

Table 3: Limiting cases of dehydration model

Limiting Case	Differential Form	Solution
Mass transfer limited	$\frac{dC_{\ell OH}}{dt} = -\frac{kA_V}{1-\phi} C_{\ell OH}$	$\frac{C_{\ell OH}}{C_{\ell OH_o}} = \exp\left[-\frac{kA_V}{1-\phi} t\right]$
H_2O/OH Equilibrium limited (no Cl_2)	$\frac{dC_{\ell OH}}{dt} = \frac{-2f RT K_w^{\ 2}}{PV} C_{\ell OH}^2$	$\frac{1}{C_{\ell OH}} = \frac{1}{C_{\ell OH_o}} + \frac{2f K_w^{\ 2} RT t}{PV(1-\phi)}$
H_2O/OH Equilibrium limited (high Cl_2 levels and $C_{gCl_2} >> C_{gH_2O}$)	$\frac{dC_{\ell OH}}{dt} = -\frac{f RT K_w}{PV(1-\phi)}\left(\frac{K_d C_{gCl_2}^{\ 2}}{C_{gO_2}}\right)^{1/4} C_{\ell OH}$	$\frac{C_{\ell OH}}{C_{\ell OH\,o}} = \exp\left[\frac{-f RT K_w}{PV(1-\phi)}\left(\frac{K_d C_{gCl_2}^{\ 2}}{C_{gO_2}}\right)^{1/4} t\right]$

5. DISCUSSION

5.1 Application of the dehydration model to small scale melts

Using the determined or literature values for $D_{\ell OH}$, K_{wp}, and K_d as a function of temperature, the known melt properties, and the known experimental parameters (see Table 4), the full dehydration model (described in Section 4) was used to compute the OH removal rates from LG-770 melts. Two values that are not well known, the OH extinction coefficient (ε) and L_s were used as fitting parameters in the model. Limits on reasonable values were set for both of these parameters. The extinction coefficient relates the absorption coefficient of OH at 3.333 μm to the OH concentration in the glass in ppm by weight. Reported values for the OH extinction coefficient vary from about 30 to 400 ppm/cm^{-1} with most factors ranging from 50 to 130 ppmw/cm^{-1} [15]. The H_2O/OH extinction coefficient that best fits the data was determined to be 52 ppmw/cm^{-1} (see Table 4).

The value of the other fitting parameter, L_s, effects the relative amount of mass transfer at the bubble interface to that at the top surface. The ratio L_s/v_s (=l_s) gives the length scale over which a packet of fluid is assumed to remain on the surface. The value of L_s found during the fitting procedure results in values of l_s on the order of 1 cm. One would expect the length scale to be bounded by the diameter of the vessel at the high end and the characteristic bubble size at the low end, and, indeed, the determined values of l_s fit within these bounds.

A similar fitting procedure was performed for LHG-8, except that values for $D_{\ell OH}$ were not available. Assuming that the H_2O/OH extinction coefficient (ε) is the same for both glasses, the data was fit using two fitting parameters ($D_{\ell OH}$ and L_s). The $D_{\ell OH}$ values that best fit the data were $D_{\ell OH} = 2.0 \times 10^{-11}$ m^2/sec (1000°C), 3.0×10^{-11} m^2/sec (1100°C), and 4.3×10^{-11} m^2/sec (1165°C). Note that different combinations of $D_{\ell OH}$ and L_s can be used to fit the data; however the values we ultimately chose appear to reasonably fit both the small-scale test melts and large-scale continuous production melts the best (see section 5.5).

Table 4. Parameters used in dehydration model

	LG-770	LHG-8
Experimental Parameters		
Column diam. (d_c)	9.4 cm	11.2 cm
Column height	17 cm or 9.5 cm	12.7 cm
Cover gas (f_c)	20 scfh	0
Temperature (T)	1200-1300°C	1000-1165°C
Flow rate (f)	0-1.08 scfh	0.54-1.1 scfh
Melt Parameters		
Viscosity (μ_ℓ)	0.30 Pa • sec	0.96 Pa • sec
Surface tension (σ)	0.15 N/m	0.15 N/m
Melt density (ρ_ℓ)	2.12 g/cm^3	2.32 g/cm^3
K_d	Eq. (10)	Eq. (10)
K_{wp}	Eq. (7)	Eq. (7)
$D_{\ell OH}$	Eq (2)	**see Section 5.1***
OH extinction coefficient (ε)	**52 ppm/cm^{-1}***	52 ppm/cm^{-1}
L_s	**3×10^{-5} m^2/s***	**15×10^{-5} m^2/s***

*Used as a fitting parameter in the model

5.2 Effect of experimental parameters on dehydration kinetics

To fairly compare the dehydration rates for different melts, the data in Figs. 6 and 7 are plotted in terms of the normalized OH content (i.e. α at time t over α at time zero (α_0)). In addition, a log scale abscissa is used because it best illustrates small changes over an extended range of water content. However, care should be exercised when viewing the data

on such semi-log plots so that too much weight is not given to very low values of the ratio α/α_0.

The solid lines in Figures 6a-6f represent the predictions of the full dehydration model to the data using the parameters summarized in Table 4. Considering all the plots, the fits to the data are reasonably good, remembering that all the data is shown on semi-log plots. Figure 6a illustrates the effect of temperature on the rate of dehydroxylation for LG-770 glass during bubbling with O_2 and Cl_2. The rate of dehydroxylation increases with an increase in temperature. This is not surprising since both the mass transport ($D_{\ell OH}$), and the equilibrium constraints (K_d, K_w) are driven toward values that would increase the dehydroxylation rate. However, the temperature effect is relatively small over the temperature range explored in this study. As seen in Fig. 6b, the effect of bubbling flow rate is much greater. After one hour of bubbling, a 4× increase in flow rate resulted in about a 5× improvement in the degree of dehydroxylation. Without any bubbling (i.e. where all dehydration takes place at the melt top surface), a noticeable amount of dehydration still takes place (see Fig. 6c). The addition of O_2 bubbling at 0.54 scfh (shown on the same plot) increases the amount of dehydroxylation by 7× after one hour. The addition of Cl_2 to the gas bubbling (also shown in the same plot) increases the amount of dehydroxylation by 29× after one hour (compared to no bubbling). Clearly, to achieve fast rates of dehydroxylation, the use of higher flow rates and the presence of Cl_2 are preferred.

While the OH concentration in the glass melt is still high, changing the amount of Cl_2 in the bubbling gas compositions should also have a strong effect on the amount of dehydroxylation. Remember that Cl_2 acts as a getter which chemically removes H_2O from the gas phase and increases the driving force for more OH to come out of the liquid. At low OH concentrations in the liquid, the amount of Cl_2 present does not play as strong of a role, because there is more Cl_2 than H_2O present in the gas phase. However, the presence of at least a small amount of Cl_2 is needed to enhance the rate of dehydroxylation. This is because without Cl_2, even small amount of H_2O in the vapor will saturate the gas (see Eq. (5)); hence, the OH removal will be slow.

The results of the glass melts performed by bubbling at various Cl_2 concentrations are shown in Fig. 6d. The model predictions to the data are not as good for this set of experiments. The experimental data, specifically those taken with high Cl_2, show less dehydration than predicted by the model. There are two possible explanations for the data: 1) the mechanism for Cl_2 reaction is not accurate, or 2) the experimental measurements may have had error in the amount of Cl_2 that was added. Further study is required to determine the cause of this discrepancy.

Figure 6e shows the results for the dehydroxylation of the LHG-8 glass melts. Similar trends to the LG-770 melts are observed; the dehydroxylation rate increase at higher temperatures and flow rates. The initial OH content in the LHG-8 glass was about 3× higher than LG-770, and only O_2 bubbling was performed in these melts. Hence the relative amount of dehydroxylation was less than that observed with LG-770 for the same amount of bubbling time. The mass transport of OH in the LHG-8 glass melts was significantly lower than in the LG-770 ($D_{\ell OH} = 3.0\times 10^{-11}$ m^2/sec for LHG-8 and $D_{\ell OH} = 1.7 \times 10^{-9}$ m^2/sec at 1100°C). The lower diffusivity may be related to the lower viscosity of LG-770 compared to LHG-8 at equivalent temperatures (see Table 4). However, a 3× change in viscosity can not account for such a large diffusivity change (~100×). This may mean that mass transport is not driven specifically by OH diffusion, but by some other mechanism. Despite the fact that the true mechanism for OH mass transport is not well understood, the determined values for $D_{\ell OH}$ do a reasonable job at predicting OH removal rates in both small-scale melts as well as production size melts (see section 5.5).

Figure 6f illustrates the effect of melt height on the rates of dehydration. As the melt height increases, so does the volume; therefore, the dehydroxylation should decrease. Our results match this observation. Another feature of using different melt heights is that it changes the ratio of the amount of mass transport that takes place at the top surface of the melt compared to that of the bubble surfaces. So the model fit to these experiments is a good test of whether these two mass transport terms are valid. The model prediction agrees fairly well with the data suggesting that our chosen value for L_s is reasonable.

5.3 Role of cover gas and cover gas humidity

Two important considerations in the fitting the full dehydration model are the effect of using a cover gas (f_c) and the partial pressure of H_2O (P_{H_2O}) in the cover gas. Figure 7a illustrates the dehydroxylation kinetics with and without a cover gas; the difference is significant. The cover gas increases the mass transport at the top surface by decreasing $C_{\ell OH_s}$. Also, this effect is large because the melt size is small; for larger size melts, the effect of cover gas would be much smaller because the surface area to volume ratio would be much smaller.

The presence of a trace amounts of moisture in the gas supply will prevent the OH content in the glass melt from reaching zero. Without any humidity in the cover gas or bubbling gas, the model predicts the water content to drop to very low values ($\alpha/\alpha_o < 10^{-3}$) (see Fig. 7b). However, the measured OH content does not drop to such levels. A probable explanation for this behavior is that some trace amounts of H_2O are in the gas supply. The dew point of the O_2 source is –62°C (0.025 mmHg). This level of humidity still results in a much lower OH content in the glass at long times than

measured. However, a possible source of additional moisture is from ambient air leaking into the melting system. This is very possible because no provisions were present to seal the cover of the melting crucible. Knowing the humidity and temperature of the outside room air where the melts were conducted, all the data was fit to the full dehydration model by leaking a constant amount of ambient air into melting system (i.e. into the cover gas). Using 0.3% leakage of ambient air provided the best fits to the data at long times (see Fig. 7b).

5.4 Mass transfer versus equilibrium

In section 4.2.2 the analytical expressions for limiting cases in the dehydration model were derived. Figure 7c shows that the LG-770 melts were not governed by either limiting case (mass transport or equilibrium). Line 1 in Fig. 7c represents the mass transport limited case calculated using Eq. (28). Remember that this represents the case where mass transport of OH is slow enough that equilibrium is not reached. Line 2 represents the equilibrium case (Eq. (34) when Cl_2 is high and $C_{gCl_2} >> C_{gH_2O}$. Line 3 represents the full dehydration model whose calculation is described in Section 4.2. In fact the full dehydration model lies about half-way between both limiting cases for the LG770 melt (T=1200°C, f=0.54 scfh, 21.2%Cl_2). Hence, the small-scale tests can not be described solely by the limiting cases.

5.5 Simulation of large scale glass melts

The full dehydration model does a reasonable job of calculating the rate of OH removal in small-scale test melts (< 1 liter). The small-scale test melts are discontinuous or batch melts, while production scale melts are carried out by a continuous melting operation. The details of the continuous melting process are described elsewhere [1]. Continuous melting operations have the key features of using larger melt volumes and continuous melt flow through the bubble column. Both of these features increase the difficulty of removing OH from the melt.

The dehydration model has been used to predict dehydration levels for both discontinuous and continuous melting processes; in Fig. 8 the computed relative OH levels are compared to measured levels in the product glass from both melting processes. The continuous melting data represent operating regimes for which the bubbling flow rate and Cl_2 content differed by more than 10× and thus is a good test of the model. The ability to predict the dehydration in both discontinuous and continuous melts suggests that the basic model assumptions capture the primary physics and chemistry involved in dehydration of phosphate glass by gas bubbling.

6. CONCLUSIONS

The rates of dehydroxylation resulting from bubbling O_2 or Cl_2 into glass melts have been measured for two commercial laser phosphate glasses (LG-770 and LHG-8). The effect of various gas compositions, temperatures, bubbling flow rates, melt geometries, cover gas flow rates have been evaluated. A time-dependent, one-dimensional bubble column model describing dehydroxylation rates of phosphate glass melts by bubbling O_2 or O_2/Cl_2 mixtures has been utilized to describe dehydroxylation of small-scale test melts and large-scale continuous melting processes. In the model, the dehydroxylation process is governed by (1) transport of OH to the liquid/vapor interface ($D_{\ell OH}$), (2) the H_2O/OH equilibrium (K_{wp}), and (3) the equilibrium for the reverse Deacon reaction (K_d). Using measured or literature values for $D_{\ell OH}$, K_{wp}, and K_d, the model is fit to the data using two parameters ε (OH extinction coefficient (in ppm/cm^{-1})) and L_s (parameter related to the mass transfer at the top surface).

ACKNOWLEDGEMENTS

The work was performed under the auspices of the US Department of Energy by Lawrence Livermore National Laboratory under contract No. W-7405-Eng-48. The assistance of Ms. Alene Clasen in the preparation of this manuscript is greatly appreciated.

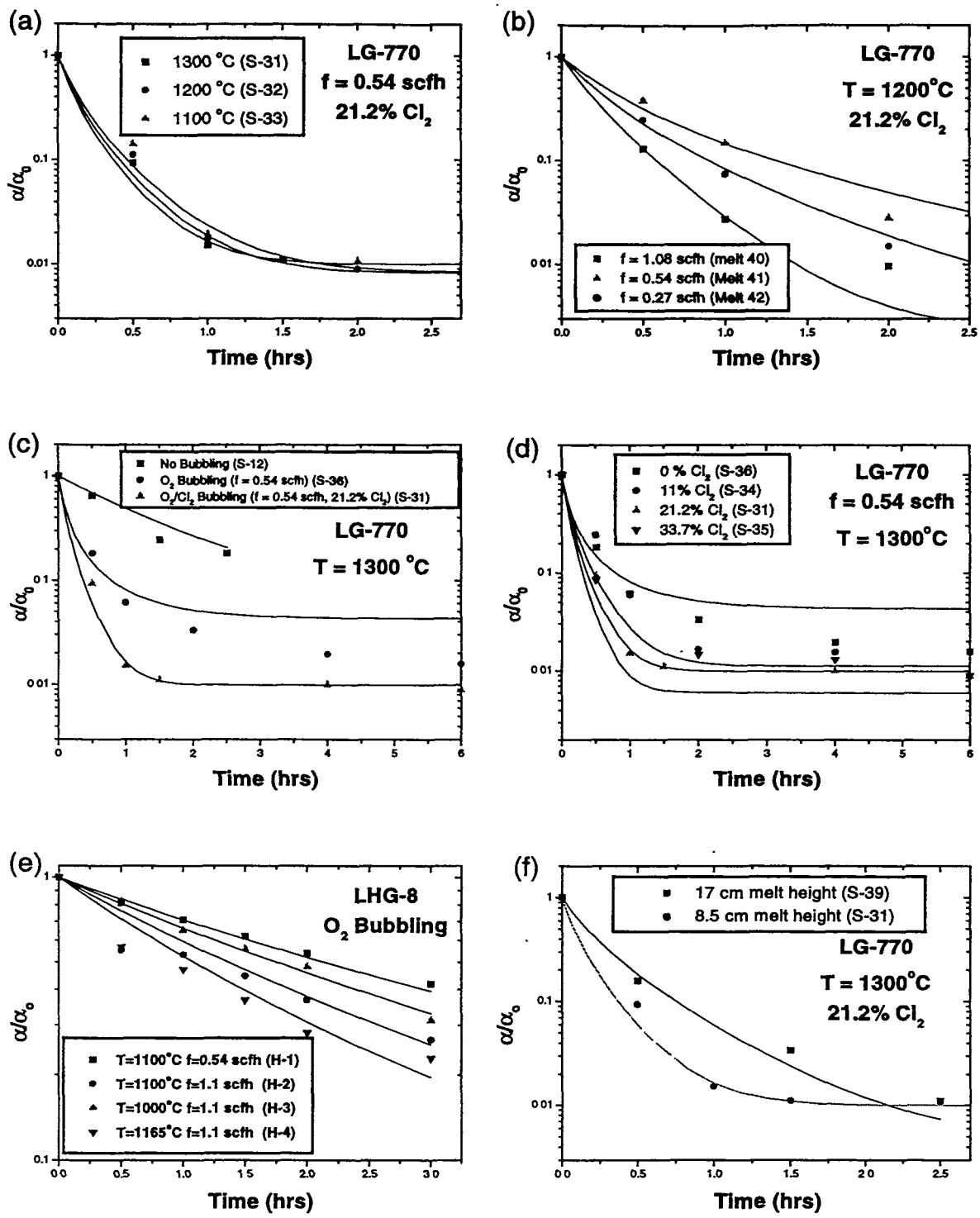

Fig. 6. Comparison of full dehydration model with experimental data. (a) Normalized OH content as function of bubbling time in LG-770 glass melts at various temperatures (f = 0.54 scfh, 21.2% Cl_2). (b) Normalized OH content as function of bubbling time in LG-770 glass melts at various bubbling flow rates (T = 1200°C, 21.2% Cl_2). (c) Normalized OH content as function of bubbling time in LG-770 glass melts at different bubbling conditions (no bubbling, 0.54 scfh (O_2 only), and 0.54 scfh (21% Cl_2)). (d) Normalized OH content as function of bubbling time in LG-770 glass melts at various Cl_2 concentrations (T=1300°C, f = 0.54 scfh, 21.2% Cl_2). (e) Normalized OH content as function of bubbling time in LHG-8 glass melts at various temperatures (1000 to 1165°C) and flow rates (0.54 to 1.1 scfh). (f) Normalized OH content as function of bubbling time in LG-770 glass melts with different melt heights (8.5 cm and 17 cm) (T =1300°C, f= 0.54 scfh, 21.2% Cl_2).

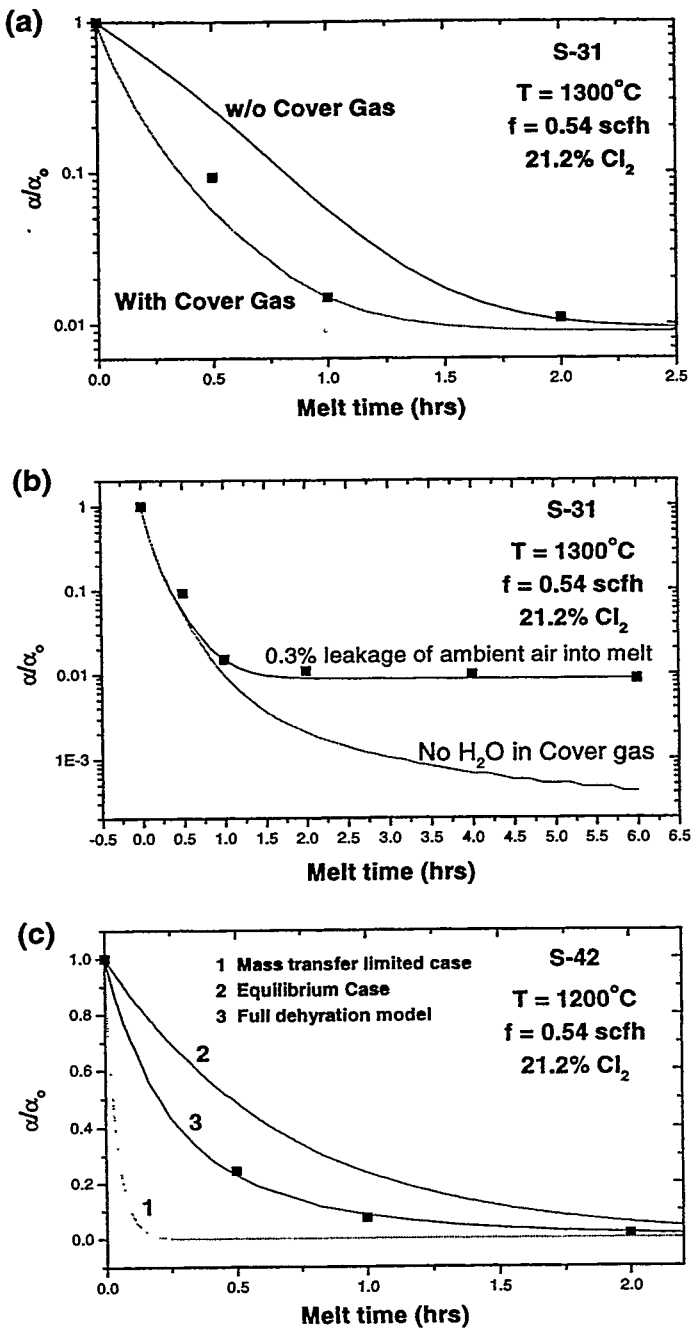

Fig. 7. (a) Normalized OH content as function of time in LG-770 glass (T= 1300°C, f = 0.54 scfh, 21.2% Cl_2). The lines represent the model fit to the data with and without cover gas. (b) Same as (a) except that the lines represent model fits to the data when no P_{H_2O} is present in the cover gas, and when P_{H_2O} is 64 Pa (i.e. 0.3% of outside air is leaking into melt system). (c) Normalized OH content as function of time in LG-770 glass (T= 1200°C, f = 0.54 scfh, 21.2 % Cl_2). Line 1 represents the mass transport limited case calculated using Eq. (28); line 2 represents equilibrium case calculated using Eq. (34); and line 3 represent full dehydration model case as described in Section 4.

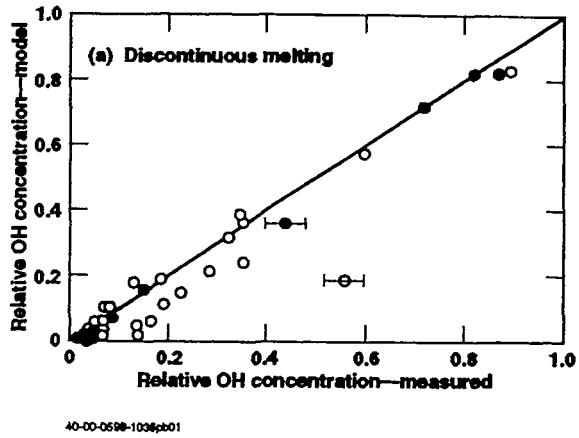

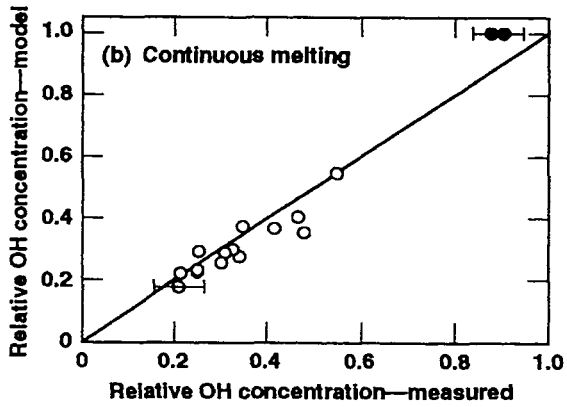

Fig. 8. Comparison of measured versus predicted OH concentrations in glass produced by (a) small-scale test melts (<1 ℓ) and (b) production-scale continuous melting operations. The solid circles are using O_2 bubbling only, while open circles represent bubbling with O_2 and variable amounts of Cl_2 (<50%).

REFERENCES

[1] J. H. Campbell, T. I. Suratwala, C. B. Thorsness, J. S. Hayden, A. J. Thorne, J. M. Cimino, A. J. Marker, K. Takeuchi, M. Smolley, and G. F. Ficini-Dorn, "Continuous Melting of Nd-doped Phosphate Laser Glasses," *J. Non-Cryst. Solids*, Vol. 263&264, pp. 342-357, 2000.

[2] J. H. Campbell and T. I. Suratwala, "Nd-doped Phosphate Glasses for High-Energy/ High-Peak-Power Lasers," *J. Non-Cryst. Solids*, Vol. 263&264, pp. 318-341, 2000.

[3] J. T. Rantala, S. Honkanen, and N. Peyghambarian, "Potential and Challenges of Sol-Gel Materials for Erbium-Doped Amplifiers," SPIE 3622, pp. 52-57, 1999.

[4] P. Becker, N. Olsson, and J. Simpson, *Erbium-Doped Fiber Amplifiers*. San Diego: Academic Press, 1999.

[5] M. Dejneka and B. Samson, "Rare-Earth-Doped-Fibers for Telecommunications Applications," *MRS Bulletin*, Vol. 24, 9, pp. 39-45, 1999.

[6] S. I. Najafi, "Overview of Nd- and Er- Doped Glass Integrated Optics Amplifiers and Lasers," SPIE 2996, pp. 54-61, 1997.

[7] D. W. Hewak, "Progress Towards a 1300 nm Fibre Amplifier," IEEE Colloquium New Developments in Optical Amplifiers 492, pp. 1-5, 1998.

[8] T. I. Suratwala, R. A. Steele, G. D. Wilke, J. H. Campbell, and K. Takeuchi, "Effects of OH Content, Water Vapor Pressure, and Temperature on Slow Crack Growth Behavior in Phosphate Laser Glass," *J. Non-Cryst. Solids*, Vol. 263&264, pp. 213-227, 2000.

[9] R. Adams, "Some Experiments on the Removal of Water from Glass," *Phys. Chem. Glasses*, Vol. 2, 2, pp. 50-54, 1961.

[10] J. Chun, Z. Junzhou, and Z. Dunshui, "Investigation on Removal of -OH Group in $BaO-P_2O_5$ and $R_2O-BaO-P_2O_5$ System Phosphate Laser Glasses by Means RAP Method," *Chin. J. Lasers*, Vol. A23, pp. 182-185, 1996.

[11] F. Gomez, P. Vast, P. Llewellyn, and F. Rouquerol, "Dehydroxylation Mechanisms of Polyphosphate Glasses in Relation to Temperature and Pressure," *J. Non-Cryst. Solids*, Vol. 222, pp. 415-421, 1997.

[12] T. Elmer, "Dehydroxylation of Porous Glass by Means of Chlorine," *J. Am. Ceram. Soc.*, Vol. 64, 3, pp. 150-154, 1981.

[13] T. Elmer, "Chlorine Treatment of Nitrided PorousGlass," *Glastech. Ber. Glass Sci. Technol.*, Vol. 61, 1, pp. 24-27, 1988.

[14] E. Boulos and N. Kreidl, "Water in Glass: A Review," *J. Canadian Ceram. Soc.*, Vol. 41, pp. 83-90, 1972.

[15] J. Shelby, "Water in Glasses and Melts," in *Handbook of Gas Diffusion in Solids and Melts*. Materials Park, OH: ASM International, 1996, pp. 217-234.

[16] C. J. Brinker and G. W. Scherer, *Sol-Gel Science: The Physics and Chemistry of Sol-Gel Processing*. San Diego: Academic Press, 1990.

[17] T. Elmer, "Dehydroxylation of Porous Glass by Means of Chlorine," *J. Am. Ceram. Soc.*, Vol. 64, 3, pp. 150-154, 1980.

[18] H. Ebendorff-Heidepriem, W. Seber, and D. Ehrt, "Dehydration of Phosphate Glasses," *J. Non-Cryst. Solids*, Vol. 163, pp. 74-80, 1993.

[19] S. Martin, "Review of the Structures of Phosphate Glasses," *Eur. J. Solid State Inorg. Chem.*, Vol. 28, pp. 163-205, 1991.

[20] R. M. Wenslow and K. T. Mueller, "Structural Details of Aqueous Attack on a Phosphate Glass by $^1H/^{31}P$ Cross Polarization NMR," *J. Phys. Chem. B*, Vol. 102, 45, pp. 9033-9038, 1998.

[21] M. Tomozawa, "Concentration Dependence of the Diffusion Coefficient of Water in SiO_2 Glass," *Communications of the American Ceramic Society*, September, pp. C251-C252, 1985.

[22] J. S. Hayden, M. Tomozawa, and S. Crichton, "OH Diffusion Measurements in Phosphate Laser Glasses," Schott Glass Technologies, Duryea, PA UCRL-ID-136007 (Renssealaer Polytechnic Institute), 1997.

[23] C. W. Arnold and K. A. Kobe, "Thermodynamics of the Deacon Process," *Chem. Eng. Prog.*, Vol. 48, pp. 293-266, 1952.

[24] C. Y. Wen and L. T. Fan, *Model for Flow Systems and Chemical Reactors*. New York: Marcel Dekker Inc., 1975.

[25] W. D. Deckwer and A. Schumpe, "Improved Tools for Bubble Column Reactor Design and Scale-Up," *Chem. Eng. Sci.*, Vol. 48, 5, pp. 889-991, 1993.

APPENDIX: VARIABLE LIST FOR DEHYDROXYLATION MODEL

α	=	Absorption coefficient of bulk glass at 3.333 μm (cm^{-1})
α_0	=	Absorption coefficient of bulk glass at 3.333 μm (cm^{-1}) at time zero
α_s	=	Absorption coefficient of glass melt at 3.333 μm (cm^{-1}) at liquid/vapor interface
ΔG	=	free energy for K_{wp} (kJ/mol)
σ	=	Liquid surface tension (N/m)
ϕ	=	Melt porosity or void volume
μ_ℓ	=	Viscosity of liquid (Pa sec)
ρ_ℓ	=	Density of liquid (kg/m^3)
A_b	=	Total bubble surface area per unit volume (m^{-1})
A_V	=	Effective interface area per unit volume of melt, includes bubble and top surface (m^{-1})
Bo	=	Bond number
C_g, C_ℓ	=	Concentration of a particular species in gas or liquid (mol/m^3)
C_{gCl_2}	=	Cl_2 concentration in gas phase (mol/m^3)
C_{gH_2O}	=	H_2O concentration in gas phase (mol/m^3)
C_{gHCl}	=	HCl concentration in gas phase (mol/m^3)

C_{gO_2}	=	O_2 concentration in gas phase (mol/m^3)
C_{gT}	=	Total gas concentration (mol/m^3)
C_ℓ^*	=	Concentration of a particular species at the gas/liquid interface (mol/m^3)
$C_{\ell OH}$	=	OH concentration in liquid (mol/m^3)
$C_{\ell OH_s}$	=	OH concentration at the liquid/gas bubble interface (mol/m^3)
$C_{\ell OH_o}$	=	OH concentration in liquid at time zero (mol/m^3)
D	=	Diffusivity of a generic species (m^2/sec)
d_c	=	Diameter of bubble column (m)
$D_{\ell OH}$	=	Effective diffusion coefficient for OH in liquid (m^2/sec)
E_g, E_ℓ	=	Dispersion coefficient in the gas phase and liquid phase (m^2/sec)
f	=	Bubbling gas flow rate in equilibrium with melt (mol/sec)
f_c	=	Cover gas flow rate (mol/sec)
Fr	=	Froude number
g	=	Acceleration due to gravity (m/sec^2)
Ga	=	Galilei number
k	=	mass transfer coefficient (m/sec)
K_d	=	Reverse Deacon reaction equilibrium constant (mol/m^3)
K_o	=	Pre-exponential constant for K_{wp} ($Pa^{1/2}/cm^{-1}$)
K_w	=	H_2O/OH equilibrium constant for phosphate glass ($(mol/m^3)^{1/2}$)
K_{wp}	=	H_2O/OH equilibrium constant for phosphate glass ($Pa^{1/2}/cm^{-1}$)
L_s	=	Parameter related to the characteristic length (l_s) (m^2/sec)
l_s	=	Characteristic length that relates to mass transport at surface (m)
P	=	Total gas pressure (Pa)
P_{H_2O}	=	H_2O partial pressure in the gas phase (Pa)
r_d	=	Reaction rate constant for the reverse Deacon reaction $\left(\frac{m^9}{mol^3\,\mathrm{sec}}\right)$
R	=	Ideal gas constant (8.314 J/mol • K)
R_g, R_ℓ	=	Input or removal rate of species in gas phase and liquid phase due to bulk reaction (mol/m^3 sec)
$R_{H_2O/HCl}$	=	Reaction rate of H_2O in gas phase with Cl_2 to form HCl in gas phase (mol/m^3 sec)
Sc	=	Schmidt number
Sh	=	Sherwood number
T	=	Temperature (K)
t	=	Time (sec)
U_g, U_ℓ	=	Average gas phase and liquid phase velocities (m/sec)
u_g	=	Superficial velocity (m/sec)
V	=	Melt volume (m^3)
v_s	=	Characteristic velocity that relate to mass transport at surface (m/sec)
y_{H_2O}	=	Gas mole fraction of H_2O
y_{HCl}	=	Gas mole fraction of HCl
z	=	Height in bubble column (m)